IEEE Access
Multidisciplinary | Rapid Review | Open Access Journal

Received September 25, 2020, accepted September 26, 2020, date of publication September 30, 2020,
date of current version October 9, 2020.

Digital Object Identifier 10.1109/ACCESS.2020.3027976

Enabling Capacity Estimation With Ergodic Interference Power in Cellular-Based Multiple UAV Systems

TIANXIAO ZHAO[1], JIANMING ZHOU[1], YUNFEI MA[2], AND FEI QIN[3,4], (Member, IEEE)

[1]School of Information and Electronics, Beijing Institute of Technology, Beijing 100081, China
[2]The 27th Research Institute of China Electronics Technology Group Corporation, Zhengzhou 450015, China
[3]School of Electronic and Electrical Communication Engineering, University of Chinese Academy of Sciences, Beijing 100049, China
[4]Key Laboratory of Information Technology for Autonomous Underwater Vehicles, Chinese Academy of Sciences, Beijing 100190, China

Corresponding author: Fei Qin (fqin1982@ucas.ac.cn)

This work was supported in part by the National Nature Science Foundation of China under Grant 61771047 and Grant 62071450, in part by the Scientific Instrument Developing Project of the Chinese Academy of Sciences under Grant YJKYYQ20170074, and in part by the Open Project of Key Laboratory of Information Technology for Autonomous Underwater Vehicles, Chinese Academy of Sciences.

ABSTRACT The integration of unmanned aerial vehicles (UAVs) into cellular networks as aerial user equipment (aUE) has attracted increasing interest from both academia and industry in recent years. To ensure stable uplink (UL) service performance, the potential UL capacity must be determined for a variety of communication techniques to guide the system design or to obtain an optimized solution. Unlike traditional interferences from ground UEs, which contribute to only local and nearby cells, UAV systems involve strong LoS paths to even far side base stations (BSs) due to higher altitude. As a result, intercell interference becomes the dominating factor in the estimation of the potential capacity. In this article, we propose a theoretical model on the ergodic sum power of the interference arising from all UAVs maintaining LoS paths with the target BS. The solution to this model is difficult to obtain, and is essentially rooted in the dynamic trajectories of interfering UAVs within a vast geological range. To address this problem, we divide the model into noncorrelated parts, where each part contains the interfering UAVs that are independently and identically distributed (i.i.d.). Then we utilize the ergodic method to solve the interference power of each part. Based on this, the original nonanalytical expression for the ergodic sum interference power is transformed into a solvable integration problem, and the closed-form solution is successfully derived. Simulation based experiments are conducted on both rural macro (RMa) cell and urban macro (UMa) cell scenarios. The results validate the feasibility and accuracy of the proposed model, and confirm the severe influence of the intercell interference on the UL capacity.

INDEX TERMS Unmanned aerial vehicles, cellular network, base station, uplink capacity, ergodic sum interference power.

I. INTRODUCTION

The integration of unmanned aerial vehicles (UAVs) into cellular networks has the potential to support long-term, beyond line-of-sight (LoS) communications for a wide range of UAV applications and has thus attracted considerable research attention in recent years [1]–[4]. In these scenarios, the UAVs are incorporated into the cellular network as aerial user equipment (aUE) to perform civil tasks, e.g., highway traffic monitoring [5], [6], aerial event coverage [7] and security surveillance [8]. Unlike the traditional UE, e.g., smartphones, which fetch information through the downlink (DL) stream, the UAVs in these applications act as information providers relying on the uplink (UL) stream with heavy traffic load and strict delay requirements. To fulfill the intensive data transfer requirements, multiple UAV communication techniques have been proposed based on the estimation of UL capacity. For example, capacity is the key metric in UAV data compression and transmission for choosing strategies [9], [10]. Capacity, and signal-to-interference-plus-noise ratio (SINR) which is a

The associate editor coordinating the review of this manuscript and approving it for publication was Adnan M. Abu-Mahfouz.

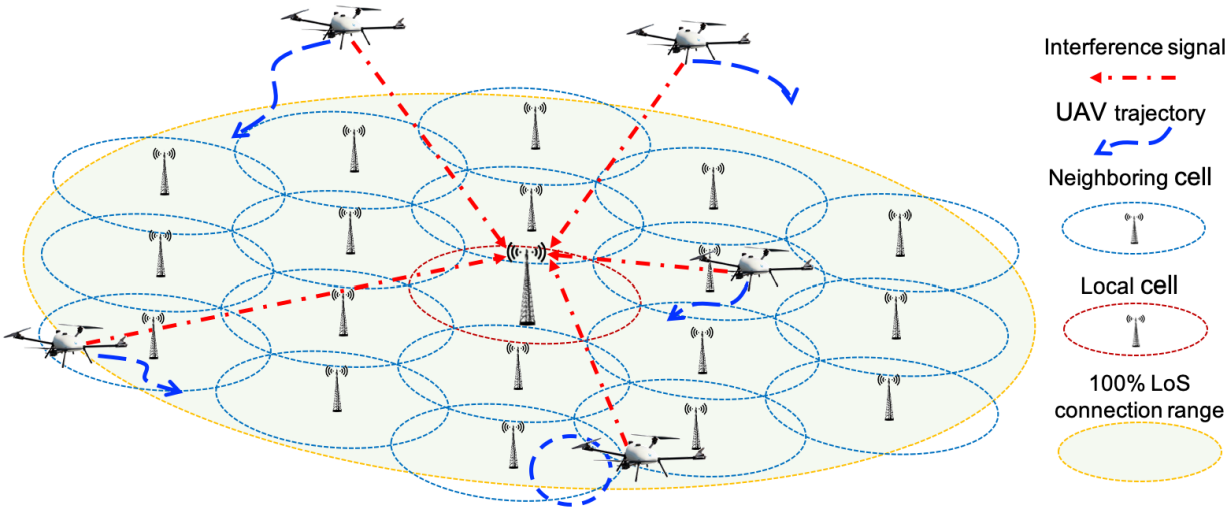

FIGURE 1. Illustration of intercell UL interference caused by LoS signals from UAVs operating in neighboring cells.

medium state parameter in calculating the capacity, are also applied in UAV power allocation and trajectory designs for performance optimization [11]–[14].

Unfortunately, the characteristics of interference necessary for estimating the SINR and potential capacity are difficult to obtain. Due to the high altitude above the ground, UAVs are likely to have strong LoS paths with nearby and even far-reaching BSs as interference sources shown in Fig. 1. This scenario gives rise to a challenging issue, where BSs are vulnerable to considerable interference from a large number of neighboring cell UAVs [15].

In a large network, UAVs occupying the same UL resources will produce continuous interference signals to the local cell BS. The total of these signals greatly affects capacity. The patterns of the UAVs' trajectories vary according to the application requirements, resulting in a random duration of connections with the target BS. Since the resources within a cell are orthogonally distributed to users, no more than one interfering UAV will exist in each cell at any moment. Therefore, these interfering UAVs are not independently and identically distributed (i.i.d.) in the geological domain. Based on the above analysis, the total intercell interference is difficult to model. To the best of the author's knowledge, most research works in this area conduct only empirical measurements on the signals from a single or multiple UAVs [15]–[21], while theoretical studies are lacking sufficient analysis with closed-form solutions [22]. A theoretical model with analytically solvable methods to precisely estimate the system-level interference remains an open issue.

To this end, we propose an ergodic model on the sum interference power, which captures the statistical properties of the signals of interfering UAVs over their dedicated movement patterns and connection durations. The proposed system model is grounded in the UAV channel model provided by the standard of the 3rd Generation Partnership Project (3GPP) [23]. To analyze the model, we first divide the region containing the interfering UAVs into noncorrelated parts, which can be analytically solved for the interference power using the ergodic method. We then transform the original non-analytical problem into a set of solvable integration problems. Finally, we obtain the solution to the sum of these integrations as the UL ergodic interference power. The proposed model provides closed-form solutions to the ergodic sum interference power for varying network conditions. This guarantees accurate estimations on the UL capacity in UAV communications. Therefore, upper-layer applications relying on the UL capacity or SINR to form the optimization problems should experience improved performance.

The rest of this article is organized as follows. Section II introduces the related works on interference and capacity in cellular-based UAV networks. Section III provides the system model and problem formulation. Section IV derives the analytical solutions of the UL ergodic sum interference power and capacity. Simulation based experiments and results are given in Section V. Finally, Section VI concludes the paper and discusses potential future work.

II. RELATED WORKS

To study UAV network interference, the LoS connectivity between the UAV and the BS and the signal propagation model must first be established. Most importantly, because the interference power is a collective effect arising from all interfering UAVs, the probabilistic geological distribution of the UAVs must be studied. Sophisticated research has been conducted on interference and capacity in traditional ground cellular networks [24]–[26], whereas much less attention has focused on cellular-based UAV communications. Meanwhile, the results of the previous works cannot be applied directly in our scenario due to the radical differences in signal propagation conditions: Rayleigh fading is assumed in the

traditional networks, whereas Rician fading is assumed in UAV communications.

Regarding the LoS connectivity in the Rician-dominated air-ground (AG) channel, the recent work of 3GPP has already provided accurate channel modeling capabilities based on comprehensive measurements [23]. In this document, general forms of path loss models and probabilistic models of LoS connections between a UAV and a BS are provided. Other measurements in real-world environments [15]–[19] have achieved results similar to the 3GPP models. Clearly, the analytical models provided in [15]–[19], [23] focus only on the connectivity between a single UAV and a BS. Network layouts containing large numbers of cells and UAVs have been constructed in [20] and [21] to study the influence of UAV interference. In [20], simulation results on the outage probability and outage time caused by intercell interference are provided. Although [20] and [21] are based on large network layouts, their measurements were performed in only specific areas; thus, the results lack universality.

Among the efforts to theoretically characterize UAV network interference and capacity, the work of [27] has provided interference modeling using stochastic theory, assuming UAVs as aerial base stations (aBSs). Although the signal propagation channels are similar, the motivations in [27] are not compatible with our studied scenario since the modeled interference is in the DL. The capacity of a UAV's UL connection to a cellular system has been studied using LoS signal transmission models in [28]–[30], with a focus on the long-term achievable SINR. Nonetheless, these studies failed to systematically model the interference from UAVs in nearby cells. A more comprehensive modeling on the sum interference assuming UAVs uniformly distributed in a spherical area is conducted in [22]. In this work, the authors propose a theoretical model for instantaneous interference signals without characterizing the ergodicity, and no analytical solution is provided.

In this article, we theoretically derive the ergodic power of UL interference signals from UAVs to a BS in the cellular-based UAV communication scenario. Compared with existing works, our study characterizes the ergodic sum interference power as a function of the key system parameters, e.g., path loss conditions, aerial user density and geological range. Our model can provide precise results when the network conditions vary. Therefore, various UAV-based applications are benefited. For example, data compression algorithms can utilize our model to estimate available capacity to properly adjust the compression ratio [9], [10], which is beneficial in two aspects. First, significant package loss and retransmission due to subcompression can be avoided, which is essential for applications requiring real-time data transfer, e.g., maritime surveillance and monitoring farmland or traffic [4], [5]. Second, such an act provides higher-quality videos and images when the bandwidth is sufficient. This enhancement then enables high-definition photography for event coverage and journalism applications [7]. Enabling the calculation of SINR and capacity also contributes to the formulation of optimization problems in multiple UAV trajectory design and power allocation algorithms [11]–[14]. These two techniques help to obtain higher throughput and optimized power consumption for UAVs executing complex tasks assisted by the BS, e.g., computational data offloading in disaster coverage [31], or providing services to ground users, e.g., hot spot service in sports events [11]. Successful execution of these tasks requires delicate operations to achieve a high transmission bandwidth and a limited power consumption. Table 1 summarizes the typical applications, their key features, and our contributions to enhance these features.

TABLE 1. Application scenarios.

Application	Key feature	Contribution
Maritime surveillance	Real-time	Package loss rate
Traffic monitoring	Real-time	Package loss rate
Farmland monitoring	Real-time	Package loss rate
Aerial event coverage and journalism	High-definition	Video/image quality
Hot spot service in sports events	High bandwidth, energy efficiency	Data rate, power consumption
Data offloading in disaster coverage	High bandwidth, energy efficiency	Data rate, power consumption

III. SYSTEM MODEL AND PROBLEM FORMULATION

We consider the intercell interference signals caused by UAVs in neighboring cells as the main interference during UL communications. Each UAV is equipped with a single omnidirectional antenna [23]. To simplify the problem formulation, the BS is assumed to have omnidirectional gains on the receiving end. This assumption is later relaxed in Section IV.

To model the systematical interference, the signal propagation properties should be characterized first. As discussed in section I, due to the clear paths in the AG channel the UAV's transmitted signal will most likely reach BSs other than its local cell, which will act as interference and pose a major challenge for the system performance. We adopt the channel model of 3GPP Release 15 [23], according to which the probability of LoS between UAVs and a local cell's BS approaches 1 for most of the altitude range. Meanwhile, the LoS component possesses more than 99.9% and 97% receiving power in rural macro (RMa) cell and urban macro (UMa) cell scenarios, respectively. Due to their high probability and strong significance, this article focuses directly on the LoS signals, which assumption is in accordance with multiple existing works in this field [11], [28], [29], [32]. The path loss model of the LoS signals for the UMa scenario, PL_U, is given as [23]:

$$PL_U = 28.0 + 22\log_{10}(d_{3D}) + 20\log_{10}(f_c), \tag{1}$$

where d_{3D} is the 3-dimensional (3-D) distance between the UAV and the BS, and f_c is the carrier signal frequency.

The path loss for the RMa scenario is denoted by PL_R, and is expressed as $PL_R = \max(23.9 - 1.8 * \log_{10}(h), 20)\log_{10}(d_{3D}) + 20\log_{10}(\frac{40\pi f_c}{3})$, where h is the

UAV's altitude [23]. As specified by the 3GPP standard the altitude range of high LoS probability is $40 - 300$ m. For this range, $\max(23.9 - 1.8\log_{10}(h), 20) = 20$. Therefore, the expression of PL_R is directly simplified as:

$$PL_R = 20\log_{10}(d_{3D}) + 20\log_{10}(\frac{40\pi f_c}{3}). \quad (2)$$

Based on Equ. (1) and Equ. (2), as well as the path loss model in [20], a general form of the path loss incorporating both the RMa and UMa models is given:

$$PL = 20\log_{10}(d_{3D}) + \alpha\log_{10}(d_{3D}) + \beta(f_c) + \gamma, \quad (3)$$

where $\beta(f_c)$ is a constant decided by f_c, and γ is an arbitrary constant; $0 \leq \alpha \leq 5$. By applying Equ. (3), a universal solution to the ergodic interference power can be derived. This channel model is capable of characterizing the system capacity with its major power, even in the presence of small-scale fading.

Based on the current UL resource allocation scheme of 4G and 5G systems, the full bandwidth is divided into a number of subchannels, or equalized variations, which are allocated to all UEs. Following the exclusivity standard for the resource allocation restrictions [33], [34], a single subchannel can be assigned to only a single user. And a uniform distribution of UL resources across all UEs is assumed [21]. Moreover, since orthogonal resources are allocated to UEs within the same cell, the local cell will not involve any interfering UAV at any given time. Hereafter, we refer to interfering UAVs as iUAVs for simplicity of discussion.

The 3-D intercell interference scenario is illustrated in Fig. 1. While the BS in the local cell is receiving data from the target UAV on a specific subchannel, multiple UAVs in the neighboring cells are simultaneously transmitting data using the same resources. These UAVs produce continuous interference to the local cell BS. Notably, the iUAVs move with independent trajectories, e.g., curves and circles, according to the application definitions. Let the instantaneous interference power be denoted by $X(t)$. $X(t)$ is the effective sum of all interference signals from iUAVs:

$$X(t) = \sum_{k=1}^{N_0(t)} 10^{\frac{Pt_k(t) - PL_k(t) + G_k(t)}{10}}, \quad k = 1, 2, \ldots, N_0(t), \quad (4)$$

where $N_0(t)$ is the instantaneous number of iUAVs. $Pt_k(t)$, expressed in dBm; $PL_k(t)$, expressed in dB; and $G_k(t)$, expressed in dB, are the transmission power, path loss and receiving gain of the BS antenna, respectively, for the k-th iUAV signal.

Furthermore, once the service of the current UAV is terminated, the UL resources are allocated to another UE in that cell. If the new UE is a ground user, then no interference will be produced since the lower altitude will restrict the formation of LoS paths to neighboring BSs. Otherwise, the interference source in the cell becomes another UAV with a new position and trajectory pattern. The fluctuations in individual UE's connection durations dictates that iUAVs with various mobility patterns emerge and disappear randomly at any time. Such effect produces a constantly varying distribution topology of iUAVs, thereby making the sum interference a complicated, time-varying random process.

TABLE 2. Definitions of parameters.

Parameter	Definition
R_l	Lower bound of 2-D UAV-BS distance
R_u	Upper bound of 2-D UAV-BS distance
H_l	Lower UAV altitude limit
H_u	Upper UAV altitude limit
N_{cell}	Number of neighboring cells
$\Omega_{cell_i}, i = 1, 2, ..., N_{cell}$	Volume of the i-th cell
$X(t)$	Instantaneous interference power
μ_I	Ergodic sum interference power
T_{total}	Total time duration
$N_0(t)$	Instantaneous number of iUAVs
N_{intf}	Total number of iUAVs
$N_i, i = 1, 2, ..., N_{cell}$	Total number of iUAVs in the i-th cell
d_{3D}	3-D distance between UAV and BS
r	2-D distance between UAV and BS
h	UAV's altitude
h_{BS}	BS's altitude
Pt	Transmission power of the UAV signal
G	BS's receiving gain to the UAV signal
PL_U	Signal path loss in the UMa scenario
PL_R	Signal path loss in the RMa scenario
PL	General signal path loss

The ergodic model has been widely utilized in analyzing the long-term system performance for both ground cellular networks and emerging UAV communication networks [25], [26], [35]. Therefore, it is straightforward to employ this methodology to model the long-term statistical property of such processes. The ergodic interference power, denoted as μ_I, can be expressed as follows:

$$\begin{aligned}\mu_I &= \lim_{T_{total}\to+\infty} \frac{1}{T_{total}} \int_0^{T_{total}} X(t)\mathrm{d}t \\ &= \lim_{T_{total}\to+\infty} \frac{1}{T_{total}} \int_0^{T_{total}} \sum_{k=1}^{N_0(t)} 10^{\frac{Pt_k(t) - PL_k(t) + G_k(t)}{10}} \mathrm{d}t, \end{aligned} \quad (5)$$

where T_{total} is the total time duration. Further analysis on μ_I leading to a closed-form solution is provided in the next section. We present the global parameters defined for the following discussion in Table 2.

IV. ERGODIC SOLUTIONS

A. ANALYTICAL ANALYSIS

Based on the discussion in the previous section, the analytical solutions would be difficult to derive for μ_I in Equ. (5) using most existing mathematical tools because of the complicated distribution patterns of iUAVs. In this subsection, we utilize the ergodic method to characterize the sum interference power as a function of multiple given parameters of the system.

To solve Equ. (5), we divide all the iUAVs involved in the calculation of μ_I into groups by their geological locations so that each group contains all iUAVs that appear in the same cell area. Note that at any moment, no more than one iUAV

exists in the i-th cell, thus, the N_i iUAVs appear subsequently during the process. Once data transmission from the j-th iUAV is terminated, the $(j+1)$-th iUAV either appears immediately or after a certain duration (e.g., when the resources of the j-th iUAV are reallocated to a ground user device and then to an aUE device after several rounds of reallocation). Let $T_{ij}(t)$ denote the connection duration of the j-th iUAV in the i-th cell, where $i = 1, 2, \ldots, N_{cell}$ and $j = 1, 2, \ldots, N_i$. Notably, $\sum_{j=1}^{N_i} T_{ij}(t) \leq T_{total}$ since sometimes there exist 0 iUAVs in a cell. Based on the above definitions, we can rewrite μ_I as:

$$\mu_I = \lim_{T_{total}\to+\infty} \frac{1}{T_{total}} \sum_{i=1}^{N_{cell}} \sum_{j=1}^{N_i} \int_0^{T_{ij}} 10^{\frac{Pt_{ij}(t)-PL_{ij}(t)+G_{ij}(t)}{10}} \mathrm{d}t, \tag{6}$$

where $Pt_{ij}(t), PL_{ij}(t)$ and $G_{ij}(t), i = 1, 2, \ldots, N_{cell}, j = 1, 2, \ldots, N_i$, are the transmitting power, the path loss and the gain of the j-th iUAV signal in the i-th cell, respectively. We further use α_i, $i = 1, 2, \ldots, N_{cell}$, to denote the expression of each part, which leads to the following form of μ_I:

$$\mu_I = \sum_{i=1}^{N_{cell}} \alpha_i, \tag{7}$$

where α_i is expressed as follows:

$$\alpha_i = \lim_{T_{total}\to+\infty} \frac{1}{T_{total}} \sum_{j=1}^{N_i} \int_0^{T_{ij}} 10^{\frac{Pt_{ij}(t)-PL_{ij}(t)+G_{ij}(t)}{10}} \mathrm{d}t, \quad i = 1, 2, \ldots, N_{cell}. \tag{8}$$

Based on Equ. (8), α_i is the ergodic sum interference power of the i-th cell. Since the studied network covers a large geological area, and the iUAVs are in different cells at any moment, we assume the iUAVs are carrying out independent tasks and with independent trajectories. Therefore, according to [23], the location of any UAV in a tagged cell adheres to a uniform distribution. Furthermore, as individual UEs, the iUAVs appear subsequently in the same cell, the distributions of which are not constrained by the resource allocation strategy of the cellular system. These UAVs are therefore independent from each other and are thus i.i.d. By applying the ergodic theory proposed in [36], α_i can be calculated as,

$$\alpha_i = \mathrm{Exp}(n_i)\mathrm{Exp}_i(I), \quad i = 1, 2, \ldots, N_{cell}, \tag{9}$$

where $\mathrm{Exp}(n_i), i = 1, 2, \ldots, N_{cell}$, is the expectation of the number of iUAVs in the cell area over T_{total}, and $\mathrm{Exp}_i(I), i = 1, 2 \ldots, N_{cell}$, is the expectation of the UAV interference power in the i-th cell area.

Then the relationship between N_i and N_{intf} can be written as follows:

$$\lim_{T_{total}\to+\infty} N_i = f_i \lim_{T_{total}\to+\infty} N_{intf}, \quad i = 1, 2, \ldots, N_{cell}, \tag{10}$$

where $f_i, i = 1, 2 \ldots, N_{cell}$, is a multiplication factor. Although the aUE rates vary over time on a large time scale, all cells should have identical average aUE rates which guarantees the equal density of iUAVs across the whole region where they exist. Based on the signal propagation conditions and the fact that the local cell contains no iUAVs, this region is defined by the local cell boundary (as the inner boundary), the 2-D distance range of high LoS probability (as the outer boundary), and the corresponding altitude range defined by 3GPP Release 15. Thus, f_i is the ratio between the volume of the i-th cell within the defined region Ω_{cell_i} to the volume of the entire region, Ω_R, $f_i = \frac{\Omega_{cell_i}}{\Omega_R}$. Similarly, by letting $\mathrm{Exp}(n_t)$ denote the expectation of the number of iUAVs in the defined region, $\mathrm{Exp}(n_i)$ is equal to $f_i\mathrm{Exp}(n_t)$. From the definition of $\mathrm{Exp}(n_t)$ and $\mathrm{Exp}(n_i)$, the following equation can be derived:

$$\mathrm{Exp}(n_t) = \sum_{i=1}^{N_{cell}} \mathrm{Exp}(n_i). \tag{11}$$

Since the iUAVs are uniformly distributed in a cell, according to probability theory, $\mathrm{Exp}_i(I)$ within the 3-D region of the cell area is calculated as

$$\mathrm{Exp}_i(I) = \int\int\int_\Omega \frac{1}{\Omega_{cell_i}} 10^{\frac{Pt(h,d_{3D})-PL(h,d_{3D})+G(h,d_{3D})}{10}} \mathrm{d}\sigma, \tag{12}$$

where $\frac{1}{\Omega_{cell_i}}, i = 1, 2, \ldots, N_{cell}$, is the probabilistic function of the uniform distribution of the iUAV in the i-th cell. $Pt(h, d_{3D})$, $PL(h, d_{3D})$ and $G(h, d_{3D})$ are the transmission, path loss and gain functions of the UAV altitude and 3-D distance from the local cell's BS. By substituting $f_i = \frac{\Omega_{cell_i}}{\Omega_R}$, $\mathrm{Exp}(n_i) = f_i\mathrm{Exp}(n_t)$ and Equ. (12) into Equ. (9), the expression of α_i is obtained as follows:

$$\alpha_i = \frac{\Omega_{cell_i}}{\Omega_R}\mathrm{Exp}(n_t) \int\int\int_\Omega \frac{1}{\Omega_{cell_i}} 10^{\frac{Pt(h,d_{3D})-PL(h,d_{3D})+G(h,d_{3D})}{10}} \mathrm{d}\sigma, \quad i = 1, 2, \ldots, N_{cell}. \tag{13}$$

Then, substituting Equ. (13) into Equ. (7), μ_I can be rewritten as:

$$\mu_I = \mathrm{Exp}(n_t) \sum_{i=1}^{N_{cell}} \frac{1}{\Omega_R} \int\int\int_\Omega 10^{\frac{Pt(h,d_{3D})-PL(h,d_{3D})+G(h,d_{3D})}{10}} \mathrm{d}\sigma. \tag{14}$$

Equ. (14) can be divided into two parts. The first part is $\mathrm{Exp}(n_t)$, which is defined by Equ. (11), and the second part is the rest of the expression in Equ. (14).

To derive the expression of $\mathrm{Exp}(n_t)$, we make the following deductions. First, the UAVs in the i-th cell which are expected to occupy the same resources as the target UE are denoted as $\gamma_i, i = 1, 2, \ldots, N_{cell}$. Note that if a cell is entirely contained in the defined region, then $\mathrm{Exp}(n_i) = \gamma_i$; otherwise, $\mathrm{Exp}(n_i) < \gamma_i$. Define $g_i, i = 1, 2, \ldots, N_{cell}$, as the ratio of the volume of the i-th cell within the defined region to the total volume of the i-th cell. Therefore, $\mathrm{Exp}(n_i) = g_i\gamma_i$. Let the

average number of UE devices of the i-th cell be denoted by aN_{ue}. Since UL resources are evenly allocated, the probability that a UAV is an iUAV is specified by $P_{iuav} = \frac{1}{aN_{ue}}$. Then, let the average aUE rate be denoted by aR_{aue}, which will lead to γ_i as:

$$\begin{aligned}\gamma_i &= aN_{ue}aR_{aue}P_{iuav} \\ &= aN_{ue}aR_{aue}\frac{1}{aN_{ue}} \\ &= aR_{aue}, \quad i = 1, 2, \ldots, N_{cell}. \end{aligned} \tag{15}$$

Now, the expected number of iUAVs in the i-th cell is obtained by:

$$\mathrm{Exp}(n_i) = g_i aR_{aue}, \quad i = 1, 2, \ldots, N_{cell}. \tag{16}$$

The second part of Equ. (14) is a sum of integrations each within the boundary of a cell contained in the defined region. Since these boundaries are connected, the sum of these integrations equals the integration of the whole defined region. Thus,

$$\begin{aligned}&\sum_{i=1}^{N_{cell}} \frac{1}{\Omega_R} \int\int\int_{\Omega} 10^{\frac{Pt(h,d_{3D})-PL(h,d_{3D})+G(h,d_{3D})}{10}} \mathrm{d}\sigma \\ &\quad = \frac{1}{\Omega_R} \int\int\int_{\Omega} 10^{\frac{Pt(h,d_{3D})-PL(h,d_{3D})+G(h,d_{3D})}{10}} \mathrm{d}\sigma. \end{aligned} \tag{17}$$

Finally, the analytical expression of μ_I is obtained:

$$\mu_I = (\sum_{i=1}^{N_{cell}} g_i\gamma_i) \frac{1}{\Omega_R} \int\int\int_{\Omega} 10^{\frac{Pt(h,d_{3D})-PL(h,d_{3D})+G(h,d_{3D})}{10}} \mathrm{d}\sigma. \tag{18}$$

The original expression of μ_I has been successfully transformed into a calculable integration problem, the closed-form solution of which will be provided in the next subsection.

B. DERIVATION OF CLOSED-FORM SOLUTIONS

1) ERGODIC SUM INTERFERENCE POWER

In this subsection, we solve the integration problem of Equ. (18) to obtain the final solution of μ_I. By means of simple algebra, Equ. (18) can be rewritten as:

$$\begin{aligned}\mu_I = (\sum_{i=1}^{N_{cell}} g_i\gamma_i) \frac{1}{\Omega_R} 10^{\frac{Pt}{10}} \\ \int\int\int_{\Omega} 10^{\frac{G(h,d_{3D})}{10}} \mathrm{d}\sigma \int\int\int_{\Omega} 10^{\frac{PL(h,d_{3D})}{10}} \mathrm{d}\sigma. \end{aligned} \tag{19}$$

In terms of $G(h, d_{3D})$, the BS typically applies omnidirectional gain on the receiving end. For the case of MIMO-based receiving beamforming, the average gain is still identical in any direction over long durations with the constant shifting beam directions. Therefore, $G(h, d_{3D})$ is a constant, which leads to the following equation:

$$\int\int\int_{\Omega} 10^{\frac{G(h,d_{3D})}{10}} \mathrm{d}\sigma = G_e, \tag{20}$$

where G_e is a constant.

Since it is difficult to obtain the integration output by directly substituting Equ. (3) into Equ. (19), we give the following close form expression of the path loss:

$$PL = 20\log_{10}(d_{3D}) + \alpha\log_{10}(\frac{R_u + R_l}{2}) + \beta(f_c) + \gamma. \tag{21}$$

Furthermore, since both the transmission power and the expected gain are independent [23], we assume that the transmission power is identical across the whole region. By substituting Equ. (21) and Equ. (20) into Equ. (19), the following expression of μ_I is obtained:

$$\mu_I = (\sum_{i=1}^{N_{cell}} g_i\gamma_i) \frac{1}{\Omega_R} 10^{\frac{Pt}{10}} G_e \frac{1}{(\frac{R_u+R_l}{2})^{\alpha/10}} \frac{1}{10^{(\beta(f_c)+\gamma)/10}} \nu_I, \tag{22}$$

where $\Omega_R = \pi(H_u - H_l)(R_u^2 - R_l^2)$, and $\nu_I = \int\int_{\Omega} \frac{1}{r^2+(h-h_{BS})^2} \mathrm{d}\sigma$.

Then, by applying polar coordinates to the horizontal plane, the integration in ν_I can be calculated as follows:

$$\begin{aligned}\nu_I &= \int_0^{2\pi} \mathrm{d}\theta \int_{R_l}^{R_u} r \int_{H_l}^{H_u} \frac{1}{r^2 + (h - h_{BS})^2} \mathrm{d}h\mathrm{d}r \\ &= 2\pi \int_{R_l}^{R_u} \arctan(\frac{H_u - h_{BS}}{r}) - \arctan(\frac{H_l - h_{BS}}{r}) \mathrm{d}r. \end{aligned} \tag{23}$$

To solve Equ. (23), we introduce the following lemma:

Lemma 1:

$$\int \arctan\frac{c_0}{x}\mathrm{d}x = x\arctan\frac{c_0}{x} + \frac{1}{2}c_0\ln(c_0^2 + x^2) + c_1, \tag{24}$$

where x is a positive real number, c_0 and c_1 are both arbitrary constants. The proof of this lemma is given in the Appendix. By applying Lemma 1, we obtain the expression of ν_I in Equ. (25), as shown at the bottom of the next page.

Finally, by substituting the expression of Ω_R and Equ. (25) into Equ. (22), the expression of μ_I is derived, as shown in Equ. (26), as shown at the bottom of the next page. Through these efforts, the solution of the ergodic sum interference power can easily be calculated with the derived closed-form solution, given the geological information of the defined region, the average aUE rate, and transmission power, path loss and gain functions of the UAVs.

2) UL CAPACITY

Based on the closed-form solution to the ergodic interference power proposed in the last subsection, the UL capacity can be derived as well, by assuming that the target UE in the local cell is a UAV moving along its own trajectory independently.

As strong interference due to LoS paths are presented, SINR is applied to calculate the capacity C, which is expressed as follows,

$$C = W\log_2(1 + \zeta), \tag{27}$$

where W is the subchannel bandwidth expressed in Hz and ζ is the average SINR expressed in dB. Let $Pr_t(t)$ denote the

received signal power from the target UAV. $Pr_t(t)$ is expressed in dBm. Since the target UAV and the iUAVs are independent from each other, ζ is obtained by calculating the ergodic sum interference power μ_I and the average power of the received target signal $E(Pr_t)$ separately:

$$\zeta = 10\log_{10}(\frac{E(Pr_t)}{\mu_I + P_N}), \tag{28}$$

where, P_N denotes the noise floor of the BS. Notably, $Pr_t(t)$ is determined by the UAV's real-time positions and is therefore expressed as $Pr_t(t) = Pt_t(h_t(t), d_{3D_t}(t)) - PL(h_t(t), d_{3D_t}(t)) + G_t(h_t(t), d_{3D_t}(t))$ where $h_t(t)$ and $d_{3D_t}(t)$ denote the altitude of the target UAV and the 3-D distance from the target UAV to the BS relative to time, respectively. $Pt_t(h_t(t), d_{3D_t}(t))$, expressed in dBm; $PL(h_t(t), d_{3D_t}(t))$, expressed in dB; and $G_t(h_t(t), d_{3D_t}(t))$, expressed in dB, are the transmission power, path loss and receiving gain of the target UAV, respectively. Based on [23], the target UAV experiences the same signal propagation conditions as the iUAVs. Thus, the path loss function is identical for them. $E(Pr_t)$ is then expressed by the following equation:

$$E(Pr_t) = \frac{1}{T_{total}} \int_0^{T_{total}} 10^{\frac{Pt_t(h_t(t),d_{3D_t}(t)) - PL(h_t(t),d_{3D_t}(t)) + G_t(h_t(t),d_{3D_t}(t))}{10}} \mathrm{d}t. \tag{29}$$

According to the industrial standard, a civil UAV's real-time positions should be reported to the ground controllers for safety concerns [4]. Therefore, $E(Pr_t)$ can be obtained by the processor as a constant determined by the target UAV's trajectory, or be known as a prior constraint by the upper layer algorithms.

Through the above analytical analysis, the final expression of C is obtained,

$$C = W\log_2(1 + 10\log_{10}(\frac{E(Pr_t)}{\mu_I + P_N})), \tag{30}$$

where μ_I is specified by Equ. (26). From the above calculations, the capacity can be obtained via Equ. (30) given the noise level and gain type of the BS receiving antenna array and the target UAV's trajectory.

The proposed closed-form solution is of low computational complexity to the mainstream processors of civil UAVs, with less than 150 adding and 200 multiplying instructions, depending on the number of cells included. Based on the default CPU frequency of DJI MATRIC 300 series, which is between 2.40 and 2.48 GHz, we estimate that the time cost of executing our proposed solution without applying any computational optimization methods is less than 5 microseconds. Therefore, this model is sufficient to be employed by most optimization algorithms in varying UAV applications.

V. SIMULATION RESULTS

This section validates the feasibility and accuracy of the proposed analytical model through simulation-based experiments. A simulation system is defined with hexagonally shaped cells [37]. Within this region, a number of random iUAVs are generated. The key simulation parameters are summarized in Table 3. The basic assumptions on the network layout are based on the settings of [23], including number of UEs in each cell, aUE rate, 2-D upper boundary, UAV's speed and altitude range, and BS's altitude. To both get the full vision of the target (or the target area) and clear photography, the UAV's altitude should be neither too low nor too high. Based on 3GPP's specifications, the altitude ranges are set to $40 - 300$ m and $100 - 300$ m for the RMa and UMa scenarios, respectively. The radius ranges of the local cell and the neighboring cells are set to $1000 - 2500$ m and $600 - 1200$ m for the RMa scenario and the UMa scenario, respectively. We apply the results of [21] by assuming that the bandwidth allocated to the UAV is 10 MHz with a transmission power of 23 dBm. The height-dependent small scale fading models of both the RMa and UMa signals are added based on the second alternative model in [23]. We choose 3 mins and 30 mins as the lower and upper duration bounds,

$$\begin{aligned} \nu_I = 2\pi(&R_u\arctan\frac{H_u - h_{BS}}{R_u} + \frac{H_u - h_{BS}}{2}\ln(R_u^2 + (H_u - h_{BS})^2) - R_u\arctan\frac{H_l - h_{BS}}{R_u} - \frac{H_l - h_{BS}}{2} \\ &\ln(R_u^2 + (H_l - h_{BS})^2) - R_l\arctan\frac{H_u - h_{BS}}{R_l} - \frac{H_u - h_{BS}}{2}\ln(R_l^2 + (H_u - h_{BS})^2) + R_l\arctan\frac{H_l - h_{BS}}{R_l} \\ &+ \frac{H_l - h_{BS}}{2}\ln(R_l^2 + (H_l - h_{BS})^2)). \end{aligned} \tag{25}$$

$$\begin{aligned} \mu_I = (&\sum_{i=1}^{N_{cell}} g_i\gamma_i)\frac{2}{(H_u - H_l)(R_u^2 - R_l^2)} 10^{\frac{P_t}{10}} G_e \frac{1}{(\frac{R_u + R_l}{2})^{\alpha/10}} \frac{1}{10^{(\beta(f_c)+\gamma)/10}} (R_u\arctan\frac{H_u - h_{BS}}{R_u} + \frac{H_u - h_{BS}}{2} \\ &\ln(R_u^2 + (H_u - h_{BS})^2) - R_u\arctan\frac{H_l - h_{BS}}{R_u} - \frac{H_l - h_{BS}}{2}\ln(R_u^2 + (H_l - h_{BS})^2) - R_l\arctan\frac{H_u - h_{BS}}{R_l} \\ &- \frac{H_u - h_{BS}}{2}\ln(R_l^2 + (H_u - h_{BS})^2) + R_l\arctan\frac{H_l - h_{BS}}{R_l} + \frac{H_l - h_{BS}}{2}\ln(R_l^2 + (H_l - h_{BS})^2)). \end{aligned} \tag{26}$$

TABLE 3. Simulation parameters.

Parameter	Value (RMa scenario)	Value (UMa scenario)
2-D upper boundary	10 km	4km
2-D lower boundary	Local cell boundary	Local cell boundary
Number of neighboring cells	$30-124$	$16-58$
Lower altitude limit	40 m	100 m
Upper altitude limit	300 m	300 m
Simulation duration	3 mins, 10 mins, 30 mins	3 mins, 10 mins, 30 mins
Individual UAV connection duration	$0-24$ s	$0-24$ s
Cell shape	Hexagon	Hexagon
Number of UEs per cell	20	20
aUE rate	$10\%-90\%$	$10\%-90\%$
Number of aUEs per cell	2-18	2-18
Individual iUAV probability	$\frac{1}{20}$	$\frac{1}{20}$
BS antenna altitude	35 m	25 m
UAV mobility model	Random walk	Random walk
UAV velocity	$30-160$ km/h	$30-160$ km/h
Azimuth angle of UAV velocity	$0°-360°$	$0°-360°$
Polar angle of UAV velocity	$-60°-60°$	$-60°-60°$
Subchannel bandwidth	10 MHz	10 MHz
UAV transmission power	23 dBm	23 dBm
BS antenna's noise power	-95 dBm	-95 dBm
Receiving gain	Uniform	Uniform
Carrier frequency	0.8 GHz	2.8 GHz
Path loss parameters	$\alpha=0, \beta=20\log_{10}(\frac{40\pi f_c}{3})$ and $\gamma=0$	$\alpha=2, \beta=20\log_{10}(f_c)$ and $\gamma=28$
Fast fading model	The second alternative in [23]	The second alternative in [23]
Rician K-factor	$22.550\log_{10}(h)-4.72$	$4.217\log_{10}(h)+5.787$

and 10 mins is chosen to exhibit the medium state. Based on a large number of tests, these three durations are sufficient to show the trend of the theoretically calculated ergodic sum interference power values compared with the experimental results.

Each UE has an equal probability of occupying the same subchannel with the local cell. If an iUAV exists in a cell, its position within the 3-D cell area is generated following a uniform distribution. Specially, for the outer-edge cells, if an iUAV is generated outside of the defined upper limit of the 2-D distance, the UAV model does not produce interference.

We use a random-walk model to represent the movement of each UAV [38]. During an individual UAV's existence, its velocity is randomly regenerated 10 times within the value and direction ranges specified in Table 3. Each iUAV moves within the bounds of the defined region. If it reaches the boundary, the process of randomly generating velocities is executed recursively until a new velocity that keeps the UAV in the region is generated. A 2-D illustration of the cell distribution and the generated UAVs' tracks are shown in Fig. 2. The figure is obtained assuming a 50% aUE rate of each cell in the RMa scenario, and the cell radius is 1500 m. The area in light green represents the 2-D range where the iUAVs are generated. In the area it shows the 2-D trajectories displayed in red of all iUAVs appeared within 45 s.

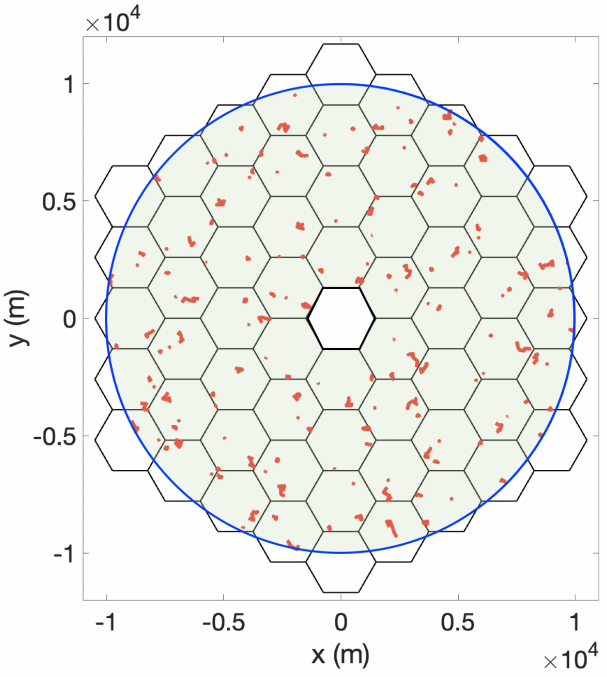

FIGURE 2. 2-D horizontal illustration of the network layout and the trajectories of the generated iUAVs.

A. ROOT MEAN SQUARE ERROR (RMSE) PERFORMANCE

The accuracy of the proposed analytical models with various aUE rates and simulation durations is verified in this subsection. Three groups of experiments are performed, each repeated 40 times for the selected durations. In Fig. 3 - Fig. 6, the root mean square errors (RMSE) are calculated between the theoretical estimations and simulation results. In each figure, cells with low, medium and high aUE densities are examined for aUE rates of 10%, 50% and 90%. We set the cell radius to 1500 m for the RMa scenario and 800 m for the UMa scenario [20], [39]. While typical UAV data

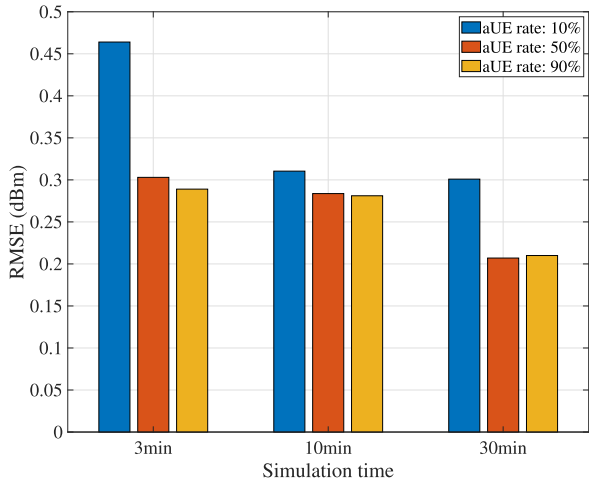

FIGURE 3. RMSE of the theoretical results compared with the experimental results versus simulation durations of the RMa scenario. Each iUAV model exists randomly for between 0 and 24 s.

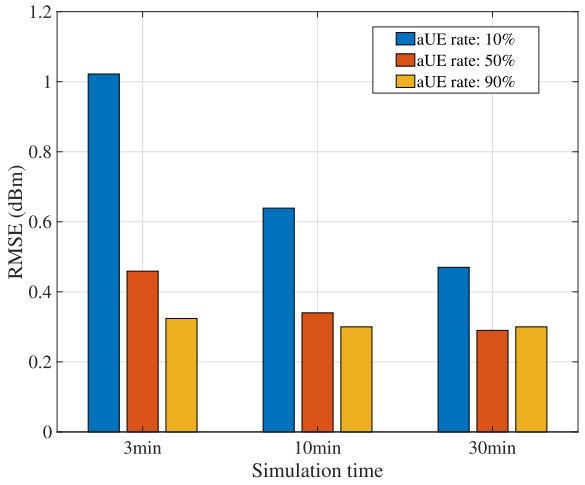

FIGURE 4. RMSE of the theoretical results compared with the experimental results versus simulation durations of the UMa scenario. Each iUAV model exists randomly for between 0 and 24 s.

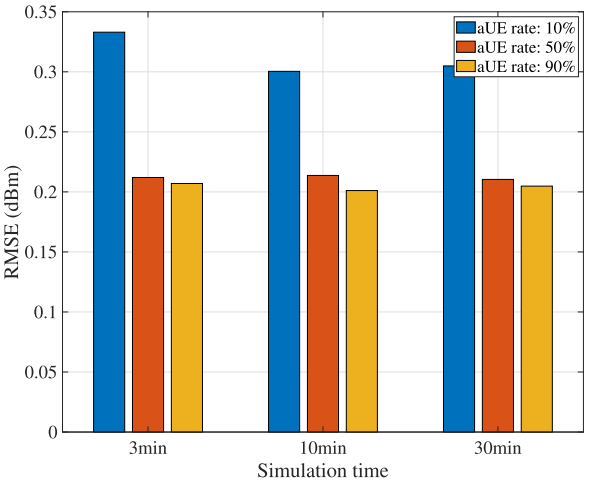

FIGURE 5. RMSE of the theoretical results compared with the experimental results versus simulation durations of the RMa scenario. Each iUAV model exists randomly for between 0 and 2 s.

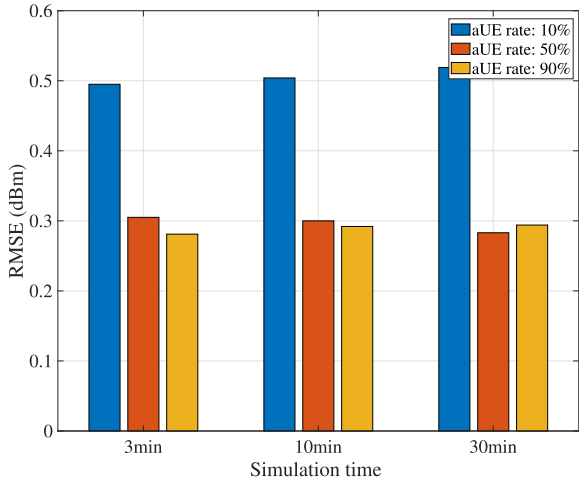

FIGURE 6. RMSE of the theoretical results compared with the experimental results versus simulation durations of the UMa scenario. Each iUAV model exists randomly for between 0 and 2 s.

transmission durations [40] are applied in Fig. 3 and Fig. 4, short-term transmission cases, where the duration is between 0 and 2 s [20], are considered in Fig. 5 and Fig. 6.

As expected, the overall RMSE values are very small for both the RMa and UMa scenarios, which validates the accuracy of the proposed closed-form solutions. After 30 mins of simulation, the RMSE for the 10% aUE rate is approximately 0.30 dBm and 0.47 dBm for the RMa and UMa scenarios, respectively. For the other two aUE rates, the RMSE is approximately 0.21 dBm and 0.29 dBm for the RMa and UMa scenarios, respectively. When the aUE rate is 10%, the distribution of iUAVs shows more drastic variations in the simulation experiment, which leads to slightly higher RMSE than that of the other two cases. The RMSE outputs for all aUE rates decrease as the simulation duration increases in Fig. 3 and Fig. 4. Nonetheless, for the same time, the outputs are similar for all aUE rates and durations in Fig. 5 and Fig. 6, which means fast convergence can be expected in these scenarios.

To summarize, we conclude that over a sufficiently long time, the theoretical model yields a stable performance for varying aUE rate cases in both the RMa and UMa scenarios. On the other hand, when UAVs and BSs maintain short-term connections, the analytical results are more accurate for short simulation durations. Furthermore, the channel model employed in the simulations includes small-scale fading, which validates the representativeness of our proposed analytical model.

B. ERGODIC SUM INTERFERENCE POWER OVER TIME

As the UL resources are allocated to the iUAVs whose trajectories and topology are constantly varying, in this subsection, the real-time calculated ergodic sum interference power is obtained and compared with the theoretical results. We set each UAV to randomly exist for between 0 and 24 s. The cell radii are 1500 m and 800 m for the RMa and UMa scenarios, respectively. The total simulation duration is 30 mins, and the

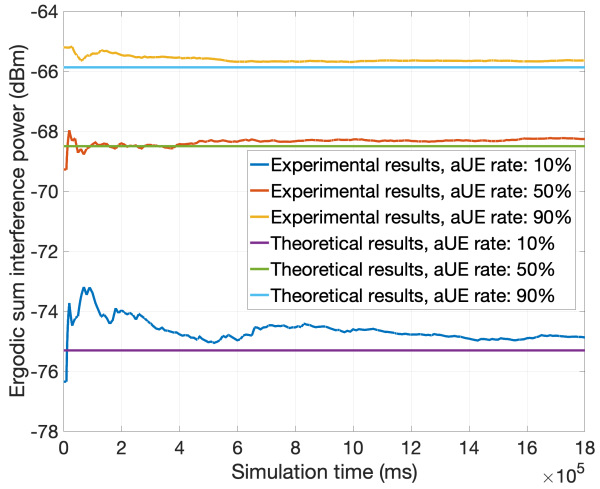

FIGURE 7. The ergodic sum interference power versus time duration of the RMa scenario.

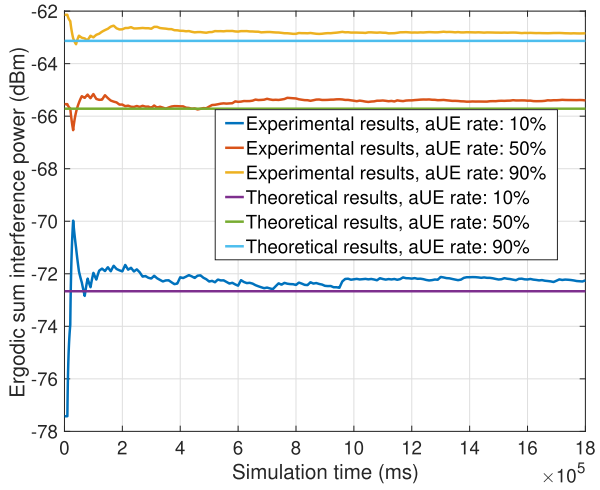

FIGURE 8. The ergodic sum interference power versus time duration of the UMa scenario.

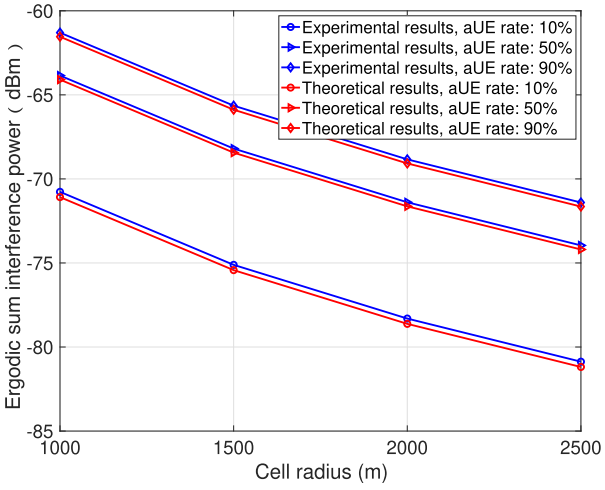

FIGURE 9. Comparison between the theoretical and experimental results of the ergodic sum interference power for varying RMa cell radii.

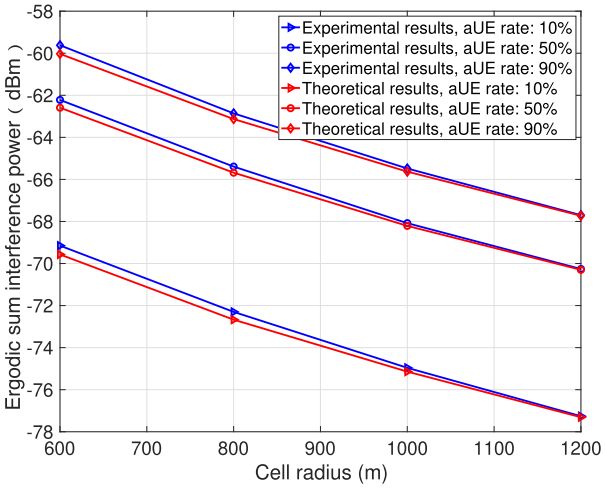

FIGURE 10. Comparison between the theoretical and experimental results of the ergodic sum interference power for varying UMa cell radii.

results are shown in Fig. 7 and Fig. 8. In both figures, three cases are considered, in which the aUE rate is chosen to be 10%, 50% or 90%.

For all three aUE rates, the experimental results converge to a constrained range. After 20 mins, the differences between the theoretical and experimental ergodic interference power results are all less than 0.40 dBm. We observe that the theoretical ergodic sum interference power is slightly lower than the experimental results. This may be due to the slightly different cell shape between the proposed theoretical model and the experimental system model. Specifically, the defined inner boundary is a circle in the theoretical model and a hexagon in the experimental model.

It can be seen that a higher aUE rate results in stronger interference in the region. For example, in Fig. 7, the theoretically calculated ergodic sum interference power reaches -65.81 dBm for the 90% aUE rate and decreases to -75.40 dBm when the aUE rate is 10%. This phenomenon is due to the fact that when more aUEs are present, there is a higher probability that a cell has an iUAV, which results in a higher number of iUAVs, and thus a stronger total interference.

C. INFLUENCE OF THE CELL RADIUS

In this subsection, the values of the interference power for various cell radii are examined. We set the aUE rate to 50% for both the RMa and UMa scenarios. A total of 5 experiments are performed for each scenario, and in each experiment, the radii of all cells are the same. The RMa cell radius varies from 500 m to 2500 m in increments of 500 m, and the UMa cell radius varies from 600 m to 1200 m in increments of 200 m. With a larger cell radius, the number of cells within the defined region is reduced. For example, in the third experiment of the RMa scenario, the cell radius is 1500 m, and 61 cells are included, while in the last experiment, where the cell radius is 2500 m, there are only 31 cells.

Fig. 9 and Fig. 10 show the ergodic sum interference power for varying local cell radii. The red lines show the experimental results obtained by averaging 20 simulations, each with

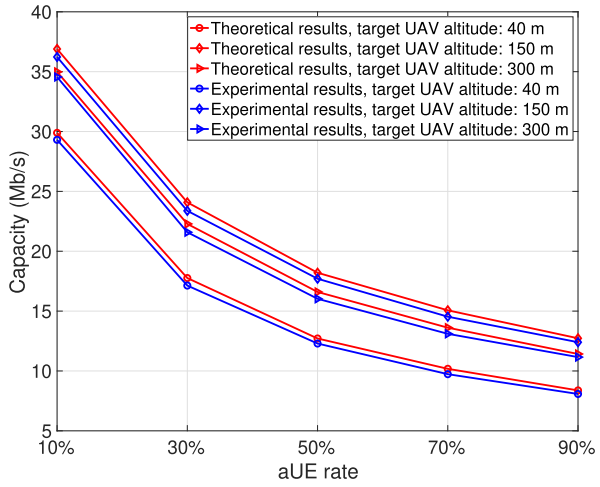

FIGURE 11. Comparison between the theoretical and experimental results of UL capacity versus aUE rates for the RMa scenario.

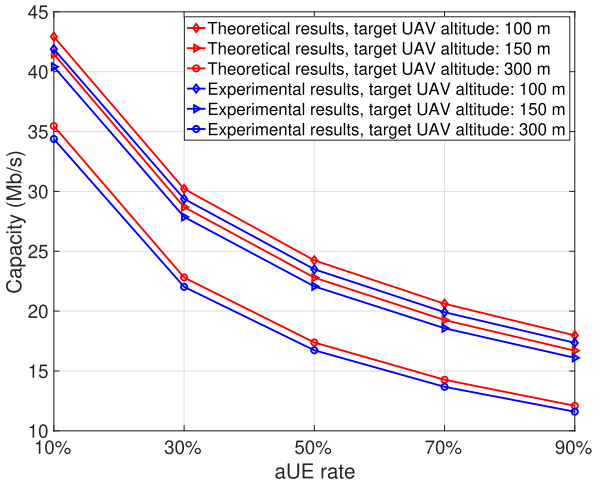

FIGURE 12. Comparison between the theoretical and experimental results of UL capacity versus aUE rates for the UMa scenario.

a duration of 30 mins. The blue lines show the theoretical results obtained directly from the proposed closed-form solution. The figures show a good match between the theoretical and experimental results, which demonstrates the accuracy of the proposed analytical model. The total ergodic interference decreases considerably as the radius increases: among all simulated scenarios, at least 19.59 dBm and 8.73 dBm margins are observed between the cases of smallest and largest radii for the RMa and UMa scenarios, respectively. This is mainly due to two reasons. First, a larger cell radius causes the average path loss to increase, thereby degrading the interference signals. Second, a larger cell radius means fewer cells are contained in the defined region. Thus, a smaller number of simultaneous iUAVs can be expected.

D. UL CAPACITY

This subsection examines the performance of the proposed analytical model in terms of capacity in various scenarios. We assume that the target signal is from a UAV being served in the local cell. The capacity values are calculated for aUE rates varying from 10% to 90% with an increment of 20%. Both the RMa and UMa scenarios are studied where the cell radii are 1500 m and 800 m, respectively. In each group of experiments, a unique position of the target UAV is chosen, with a fixed 2-D distance to the BS but varying altitude. The 2-D distance is 600 m and 300 m for the RMa and UMa scenarios, respectively. The considered altitudes are 40 m, 150 m and 300 m for the RMa scenario and 100 m, 150 m and 300 m for the UMa scenario. The experiment is executed 50 times, each with a 30 min duration, and the average capacity values are computed and compared with the theoretical results in Fig. 11 and Fig. 12.

These two figures show the accuracy of the proposed analytical model in terms of capacity with varying aUE rates and target UAV altitudes. An increase in the aUE rate causes a significant capacity degradation in both the RMa and UMa cases, i.e., theoretically 21.51 − 24.17 Mb/s and 23.31 − 24.95 Mb/s for the RMa and UMa scenarios as the aUE rate increases from 10% to 90%, respectively. Due to such a decrease in capacity, the available bandwidth for upper layer applications will also be significantly lowered. The highest capacities are obtained for the target UAV at an altitude of 150 m and 100 m in the RMa and UMa scenarios, respectively, which is a result of the lowest path loss occurring at the chosen altitudes. Clearly, these results not only validate the accuracy of the proposed model but also confirm the considerable influence of the intercell interference imposed by UAVs.

VI. CONCLUSION AND FUTURE WORKS

The widely deployed cellular networks can provide connectivity with UAVs across vast geological ranges and thus have become a potential solution for data exchange with UAVs in many applications. However, to ensure stable connections between UAVs and BSs, the UL interference problem must be addressed. In this article, we conduct a theoretical study of the ergodic sum interference power from UAVs to a BS to characterize the system-level performance in cellular networks that incorporate UAVs as aUE. To study the intercell interference imposed by iUAVs, the primary expression of the ergodic UL sum interference power is given with this geological model and the 3GPP channel model. Then, by means of the ergodic method, we derive an equivalent form of the proposed primary expression and solve the corresponding problem to obtain a closed-form solution for the ergodic sum interference power, which can easily be utilized to estimate the link capacity. Through simulation based experiments, we verify the feasibility and accuracy of the proposed analytical model, which benefits many optimization-based studies in cellular-based UAV systems.

Further verification of the proposed model based on real-world tests will be presented in future work. Other potential work includes the consideration of multiple modulation schemes and large-scale fading in the UAV channel model.

Moreover, the performance enhancement of combining the theoretical model and algorithms at the application level, e.g., adaptive video compression [41], will also be examined in our future works.

APPENDIX

Proof: The following functions are defined:

$$u(x) = \arctan\frac{c_0}{x} \tag{A.1}$$

and

$$v(x) = x. \tag{A.2}$$

Taking the first derivative of $v(x)$, we obtain,

$$\frac{\mathrm{d}v(x)}{\mathrm{d}x} = 1. \tag{A.3}$$

Then, from the properties of derivatives, the following equation is obtained:

$$\frac{\mathrm{d}(u(x)v(x))}{\mathrm{d}x} = u(x)\frac{\mathrm{d}v(x)}{\mathrm{d}x} + \frac{\mathrm{d}u(x)}{\mathrm{d}x}v(x). \tag{A.4}$$

Thus,

$$u(x)\frac{\mathrm{d}v(x)}{\mathrm{d}x} = \frac{\mathrm{d}(u(x)v(x))}{\mathrm{d}x} - \frac{\mathrm{d}u(x)}{\mathrm{d}x}v(x). \tag{A.5}$$

Applying the integration operation to Equ. (A.5),

$$\int u(x)\frac{\mathrm{d}v(x)}{\mathrm{d}x}\mathrm{d}x = \int \frac{\mathrm{d}(u(x)v(x))}{\mathrm{d}x}\mathrm{d}x - \int \frac{\mathrm{d}u(x)}{\mathrm{d}x}v(x)\mathrm{d}x, \tag{A.6}$$

which further leads to the following equation:

$$\int u(x)\mathrm{d}v(x) = u(x)v(x) - \int v(x)\mathrm{d}u(x). \tag{A.7}$$

Substituting Equ. (A.1) and Equ. (A.2) into Equ. (A.7), we obtain,

$$\begin{aligned}\int \arctan\frac{c_0}{x}\mathrm{d}x &= x\arctan\frac{c_0}{x} - \int x\mathrm{d}(\arctan\frac{c_0}{x}) \\ &= x\arctan\frac{c_0}{x} - \int -\frac{c_0 x}{x^2 + c_0^2}\mathrm{d}x \\ &= x\arctan\frac{c_0}{x} - (-\frac{1}{2}c_0\ln(x^2 + c_0^2)) + c_1 \\ &= x\arctan\frac{c_0}{x} + \frac{1}{2}c_0\ln(x^2 + c_0^2) + c_1. \end{aligned} \tag{A.8}$$

Therefore, Lemma 1 is proven. ■

REFERENCES

[1] S. Zhang, Y. Zeng, and R. Zhang, "Cellular-enabled UAV communication: A connectivity-constrained trajectory optimization perspective," *IEEE Trans. Commun.*, vol. 67, no. 3, pp. 2580–2604, Mar. 2019.
[2] Z. Xiao, P. Xia, and X.-G. Xia, "Enabling UAV cellular with millimeter-wave communication: Potentials and approaches," *IEEE Commun. Mag.*, vol. 54, no. 5, pp. 66–73, May 2016.
[3] Y. Zeng, J. Lyu, and R. Zhang, "Cellular-connected UAV: Potential, challenges, and promising technologies," *IEEE Wireless Commun.*, vol. 26, no. 1, pp. 120–127, Feb. 2019.
[4] S. Hayat, E. Yanmaz, and R. Muzaffar, "Survey on unmanned aerial vehicle networks for civil applications: A communications viewpoint," *IEEE Commun. Surveys Tuts.*, vol. 18, no. 4, pp. 2624–2661, 4th Quart., 2016.
[5] G. Granlund, K. Nordberg, J. Wiklund, P. Doherty, E. Skarman, and E. Sandewall, "Witas: An intelligent autonomous aircraft using active vision," in *Proc. Int. Tech. Conf. Exhib. (UAV)*, Paris, France, Jun. 2000, pp. 1–42.
[6] S. Srinivasan, H. Latchman, J. Shea, T. Wong, and J. McNair, "Airborne traffic surveillance systems: Video surveillance of highway traffic," in *Proc. ACM 2nd Int. Workshop Video Surveill. Sensor Netw. (VSSN)*, 2004, pp. 131–135.
[7] E. Natalizio, R. Surace, V. Loscri, F. Guerriero, and T. Melodia, "Filming sport events with mobile camera drones: Mathematical modeling and algorithms," Hyper Articles en Ligne (HAL), Lyon, France, Tech. Rep. hal-00801126, 2012.
[8] S. O'Young and P. Hubbard, "RAVEN: A maritime surveillance project using small UAV," in *Proc. IEEE Conf. Emerg. Technol. Factory Autom. (EFTA)*, Sep. 2007, pp. 904–907.
[9] K. Sayood, *Introduction to Data Compression*. San Mateo, CA, USA: Morgan Kaufmann, 2017.
[10] X.-L. Chen, S.-C. Zhang, and J. Liu, "Design of UAV video compression system based on H.264 encoding algorithm," in *Proc. Int. Conf. Electron. Mech. Eng. Inf. Technol.*, Aug. 2011, pp. 2619–2622.
[11] Y. Huang, W. Mei, J. Xu, L. Qiu, and R. Zhang, "Cognitive UAV communication via joint maneuver and power control," *IEEE Trans. Commun.*, vol. 67, no. 11, pp. 7872–7888, Nov. 2019.
[12] Q. Wu, J. Xu, and R. Zhang, "Capacity characterization of UAV-enabled two-user broadcast channel," *IEEE J. Sel. Areas Commun.*, vol. 36, no. 9, pp. 1955–1971, Sep. 2018.
[13] Y. Cai, Z. Wei, R. Li, D. W. K. Ng, and J. Yuan, "Joint trajectory and resource allocation design for energy-efficient secure UAV communication systems," *IEEE Trans. Commun.*, vol. 68, no. 7, pp. 4536–4553, Jul. 2020.
[14] Y. Sun, D. Xu, D. W. K. Ng, L. Dai, and R. Schober, "Optimal 3D-trajectory design and resource allocation for solar-powered UAV communication systems," *IEEE Trans. Commun.*, vol. 67, no. 6, pp. 4281–4298, Jun. 2019.
[15] A. Al-Hourani and K. Gomez, "Modeling cellular-to-UAV path-loss for suburban environments," *IEEE Wireless Commun. Lett.*, vol. 7, no. 1, pp. 82–85, Feb. 2018.
[16] X. Lin, V. Yajnanarayana, S. D. Muruganathan, S. Gao, H. Asplund, H.-L. Maattanen, M. Bergstrom, S. Euler, and Y.-P.-E. Wang, "The sky is not the limit: LTE for unmanned aerial vehicles," *IEEE Commun. Mag.*, vol. 56, no. 4, pp. 204–210, Apr. 2018.
[17] R. Amorim, H. Nguyen, P. Mogensen, I. Z. Kovacs, J. Wigard, and T. B. Sorensen, "Radio channel modeling for UAV communication over cellular networks," *IEEE Wireless Commun. Lett.*, vol. 6, no. 4, pp. 514–517, Aug. 2017.
[18] H. C. Nguyen, R. Amorim, J. Wigard, I. Z. Kovacs, and P. Mogensen, "Using LTE networks for UAV command and control link: A rural-area coverage analysis," in *Proc. IEEE 86th Veh. Technol. Conf. (VTC-Fall)*, Sep. 2017, pp. 1–6.
[19] K. Wang, R. Zhang, L. Wu, Z. Zhong, L. He, J. Liu, and X. Pang, "Path loss measurement and modeling for low-altitude UAV access channels," in *Proc. IEEE 86th Veh. Technol. Conf. (VTC-Fall)*, Sep. 2017, pp. 1–5.
[20] H. C. Nguyen, R. Amorim, J. Wigard, I. Z. Kovacs, T. B. Sorensen, and P. E. Mogensen, "How to ensure reliable connectivity for aerial vehicles over cellular networks," *IEEE Access*, vol. 6, pp. 12304–12317, 2018.
[21] R. Amorim, H. Nguyen, J. Wigard, I. Z. Kovacs, T. B. Sorensen, D. Z. Biro, M. Sorensen, and P. Mogensen, "Measured uplink interference caused by aerial vehicles in LTE cellular networks," *IEEE Wireless Commun. Lett.*, vol. 7, no. 6, pp. 958–961, Dec. 2018.
[22] E. Chu, J. M. Kim, and B. C. Jung, "Interference modeling and analysis in 3-dimensional directional UAV networks based on stochastic geometry," *ICT Express*, vol. 5, no. 4, pp. 235–239, Dec. 2019.
[23] *Enhanced LTE Support for Aerial Vehicles*, document 3GPP TR 36.777. [Online]. Available: ftp://www.3gpp.org/specs/archive/36_series/36.777
[24] M. Moinuddin and I. Naseem, "A simple approach to evaluate the Ergodic capacity and outage probability of correlated Rayleigh diversity channels with unequal signal-to-noise ratios," *EURASIP J. Wireless Commun. Netw.*, vol. 2013, no. 1, p. 20, Dec. 2013.
[25] G. Farhadi and N. Beaulieu, "On the ergodic capacity of wireless relaying systems over Rayleigh fading channels," *IEEE Trans. Wireless Commun.*, vol. 7, no. 11, pp. 4462–4467, Nov. 2008.
[26] C. Xiao and Y. R. Zheng, "Ergodic capacity, capacity distribution and outage capacity of MIMO time-varying and frequency-selective Rayleigh fading channels," in *Proc. Annu. Allerton Conf. Commun. Control Comput.*, vol. 41, Sep. 1998, pp. 346–355.

[27] A. Al-Hourani, "Interference modeling in low-altitude unmanned aerial vehicles," *IEEE Wireless Commun. Lett.*, early access, Jul. 14, 2020, doi: 10.1109/LWC.2020.3009302.
[28] P. Chandhar, D. Danev, and E. G. Larsson, "Massive MIMO as enabler for communications with drone swarms," in *Proc. Int. Conf. Unmanned Aircr. Syst. (ICUAS)*, Jun. 2016, pp. 347–354.
[29] P. Chandhar, D. Danev, and E. G. Larsson, "On the outage capacity in massive MIMO with line-of-sight," in *Proc. IEEE 18th Int. Workshop Signal Process. Adv. Wireless Commun. (SPAWC)*, Jul. 2017, pp. 1–6.
[30] F. A. P. de Figueiredo, C. F. Dias, E. R. de Lima, and G. Fraidenraich, "Capacity bounds for dense massive MIMO in a line-of-sight propagation environment," *Sensors*, vol. 20, no. 2, p. 520, Jan. 2020.
[31] F. Zhou, R. Q. Hu, Z. Li, and Y. Wang, "Mobile edge computing in unmanned aerial vehicle networks," *IEEE Wireless Commun.*, vol. 27, no. 1, pp. 140–146, Feb. 2020.
[32] Y. Zeng, R. Zhang, and T. J. Lim, "Throughput maximization for UAV-enabled mobile relaying systems," *IEEE Trans. Commun.*, vol. 64, no. 12, pp. 4983–4996, Dec. 2016.
[33] I. Wong, O. Oteri, and W. Mccoy, "Optimal resource allocation in uplink SC-FDMA systems," *IEEE Trans. Wireless Commun.*, vol. 8, no. 5, pp. 2161–2165, May 2009.
[34] H. Myung, J. Lim, and D. Goodman, "Single carrier FDMA for uplink wireless transmission," *IEEE Veh. Technol. Mag.*, vol. 1, no. 3, pp. 30–38, Sep. 2006.
[35] P. Chandhar, D. Danev, and E. G. Larsson, "On ergodic rates and optimal array geometry in line-of-sight massive MIMO," in *Proc. IEEE 17th Int. Workshop Signal Process. Adv. Wireless Commun. (SPAWC)*, Jul. 2016, pp. 1–35.
[36] M. Reed, *Methods of Modern Mathematical Physics*. Amsterdam, The Netherlands: Elsevier, 2012.
[37] H. Yin, D. Gesbert, M. Filippou, and Y. Liu, "A coordinated approach to channel estimation in large-scale multiple-antenna systems," *IEEE J. Sel. Areas Commun.*, vol. 31, no. 2, pp. 264–273, Feb. 2013.
[38] A. Guillen-Perez and M.-D. Cano, "Flying ad hoc networks: A new domain for network communications," *Sensors*, vol. 18, no. 10, p. 3571, Oct. 2018.
[39] M. Weiss, "Telecom requirements for time and frequency synchronization," NIST, Gaithersburg, MD, USA, Tech. Rep., 2012. [Online]. Available: https://www.gps.gov/cgsic/meetings/2012/weiss1.pdf
[40] F. Wu, D. Yang, L. Xiao, and L. Cuthbert, "Energy consumption and completion time tradeoff in rotary-wing UAV enabled WPCN," *IEEE Access*, vol. 7, pp. 79617–79635, 2019.
[41] Y. Mi, C. Luo, G. Min, W. Miao, L. Wu, and T. Zhao, "Sensor-assisted global motion estimation for efficient UAV video coding," in *Proc. IEEE Int. Conf. Acoust., Speech Signal Process. (ICASSP)*, May 2019, pp. 2237–2241.

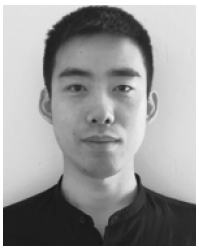

TIANXIAO ZHAO received the B.Eng. degree from the Beijing Institute of Technology, China, in 2013. He is currently pursuing the Ph.D. degree with the School of Information and Electronics, Beijing Institute of Technology. His research interests include unmanned aerial vehicle communications, beamforming technique, 5G communications, and wireless ad hoc networks.

JIANMING ZHOU received the Ph.D. degree in electromagnetic fields and microwave technology from the Beijing Institute of Technology. Since 2004, he has been engaged in teaching and research with the School of Information and Electronics, Beijing Institute of Technology. His research interests include transceiver module and signal processing, phased array communication and radar integration, and active phased array T/R components.

YUNFEI MA received the B.Eng. degree in information engineering from the Huazhong University of Science and Technology, Wuhan, China, in 2004. Since 2004, he has been with the 27th Research Institute of China Electronics Technology Group Corporation, and focus on the UAV system design.

FEI QIN (Member, IEEE) received the B.Eng. degree in information engineering from the Huazhong University of Science and Technology, Wuhan, China, in 2004, the M.Eng. degree in electronic engineering from the Beijing Institute of Technology, Beijing, China, in 2006, and the Ph.D. degree in electronic and electrical engineering from the University College London, London, U.K., in 2012. He served as a Product Manager with Crossbow Technology, Beijing Representative Office, from 2006 to 2008. He is currently an Associate Professor with the School of Electronic and Electrical Communication Engineering, University of Chinese Academy of Sciences, Beijing. His current research interests include the joint optimization method of wireless networks and information systems.